Chapter 4

Multiple Conformational Switches Control Co-translational Protein Targeting

A version of this chapter has been published as

X Zhang, C Schaffitzel, N Ban, S-O Shan, Proceedings of the National Academy of Sciences of the United States of America, (2009), ***106****, 1754-1759.*

4.1 Abstract

The "GTPase switch" paradigm, in which a GTPase switches between an active, GTP-bound state and an inactive, GDP-bound state through the recruitment of nucleotide exchange factors (GEFs) or GTPase activating proteins (GAPs), has been used to interpret the regulatory mechanism of many GTPases. A notable exception to this paradigm is provided by two GTPases in the signal recognition particle (SRP) and the SRP receptor (SR) that control the co-translational targeting of proteins to cellular membranes. Instead of the classical "GTPase switch", SRP and SR undergo a series of discrete conformational rearrangements during their interaction with one another, culminating in their reciprocal GTPase activation. Here, we show that this series of rearrangements during SRP–SR binding and activation provide important control points to drive and regulate protein targeting. Using real time fluorescence, we showed that the cargo for SRP – ribosomes translating nascent polypeptides with signal sequences – accelerates SRP–SR complex assembly over 100 fold, thereby driving rapid delivery of cargo to the membrane. A series of subsequent rearrangements in the SRP•SR GTPase complex provide important driving forces to unload the cargo during late stages of protein targeting. Further, the cargo delays GTPase activation in the SRP•SR complex by 8–12 fold, creating an important time window that could further improve the efficiency and fidelity of protein targeting. Thus the SRP and SR GTPases, without recruiting external regulatory factors, constitute a self-sufficient system that provides exquisite spatial and temporal control of a complex cellular process.

4.2 Introduction

SRP-mediated co-translational protein targeting delivers roughly a third of proteins to their correct subcellular destinations, including the eukaryotic endoplasmic reticulum and the bacterial plasma membrane. This pathway involves a sequential series of molecular steps *(2, 6, 7)*, including (1) recognition and loading of cargo (ribosomes translating nascent polypeptides with signal sequences) on the SRP; (2) delivery of cargo to the target membrane via complex formation between SRP and SR; (3) unloading and transfer of cargo from the SRP to the protein conducting channel (PCC); and (4) disassembly of the SRP•SR complex and recycling of free SRP and SR for subsequent rounds of protein targeting. Like many cellular processes, this complex series of molecular interactions are spatially and temporally regulated by members of the GTPase superfamily, in this case, two highly homologous and directly interacting GTPases in both the SRP and SR.

SRP and SR provide a notable exception to the 'GTPase switch' paradigm established for classical signaling GTPases (*75*). These GTPases do not exhibit substantial conformational changes depending on whether GTP or GDP is bound (*26-28*), and further, their intrinsic nucleotide exchange rates are 10^2–10^4 fold faster than those of classical GTPases (*29, 76*). Thus no external GEFs are required to switch these GTPases from the GDP- to the GTP-bound state, and the facilitation of nucleotide exchange by an external GEF cannot be the mechanism to turn these GTPases to the 'on' state. Moreover, SRP and SR reciprocally stimulate each other's GTP hydrolysis activity when they form a complex with one another (*21, 29*). Thus no external GAPs are required either to switch these GTPases from the GTP- to the GDP-bound state, and the

stimulation of GTP hydrolysis by an external GAP cannot be the mechanism to turn these GTPases to the 'off' state. In contrast, these GTPases undergo a series of discrete conformational changes driven by heterodimeric interactions between the two GTPases (figure 4.1) (*9, 20, 21, 77*). Both proteins, starting in an inactive, '*open*' conformation, quickly bind one another to form a transient '*early*' intermediate independently of GTP (figure 4.1, step 1). The presence of GTP bound at both GTPase active sites induces a conformational rearrangement in both proteins to form a stable '*closed*' complex (figure 4.1, step 2) (*9, 77, 78*). A subsequent rearrangement involving the activation loops in both proteins activates GTP hydrolysis (figure 4.1, step 3) (*9, 20*), which drives disassembly of the complex (figure 4.1, step 4) (*79*).

If these conformational rearrangements during SRP–SR binding and activation are integral to the regulatory role of these GTPases in protein targeting, then they should be responsive to the biological events they are monitoring. To test this hypothesis, we examined the effects of cargo loading on the kinetic and thermodynamic features of the SRP and SR's GTPase cycle. Our results demonstrate that the SRP and SR GTPases can use each of the conformational changes during their binding and activation cycle to sense temporal cues such as cargo loading and in response, substantially change the free energy landscape of the different conformational states in the SRP•SR GTPase complex. These cargo-induced responses allow these GTPases to drive the efficient delivery and unloading of cargo to the target membrane, and to potentially improve the fidelity of protein targeting via kinetic proofreading mechanisms.

4.3 Results

4.3.1 General Experimental Approach

To monitor the different conformational stages of the SRP•SR complex, we used fluorescence resonance energy transfer (FRET) between donor and acceptor probes incorporated on the SRP and SR. FRET provides a highly sensitive assay that allows us to detect the transient *early* intermediate (figure 4.1) (*80*). Further, this intermediate can be distinguished from the subsequent conformations because it has a lower FRET value than the *closed* and *activated* complexes (figure 4.1) (*80*). In addition, an environmentally sensitive probe, acrylodan labeled at residue 235 of SRP, detects formation of the *closed* and *activated* complexes but not the *early* intermediate (figure 4.1 and figure 4.S1), thereby simplifying kinetic and thermodynamic analyses of these later conformations. Finally, acrylodan labeled at residue 356 of SR near its catalytic loop specifically detects the *activated* complex (figure 4.1 and figure 4.S2). In addition to these fluorescent probes, mutant GTPases and GTP analogues were used to block specific rearrangements and thus isolate each conformational intermediate (*9, 21*). We can block the *early* $\rightarrow$ *closed* rearrangement by leaving out GTP (figure 4.1) (*80*); this allows us to isolate the *early* intermediate and characterize its kinetics and stability. Mutations in the catalytic loop, SRP A144W or SR A335W, allow a stable *closed* complex to form but block its rearrangement to the *activated* complex (*9, 10*). The non-hydrolyzable GTP analogue 5'-guanylylimido-diphosphate (GppNHp) allows most of the rearrangements to occur but inhibits GTP hydrolysis (*9, 21*). Using these tools, we determined how the SRP and SR GTPases use their conformational changes to respond to cargo loading.

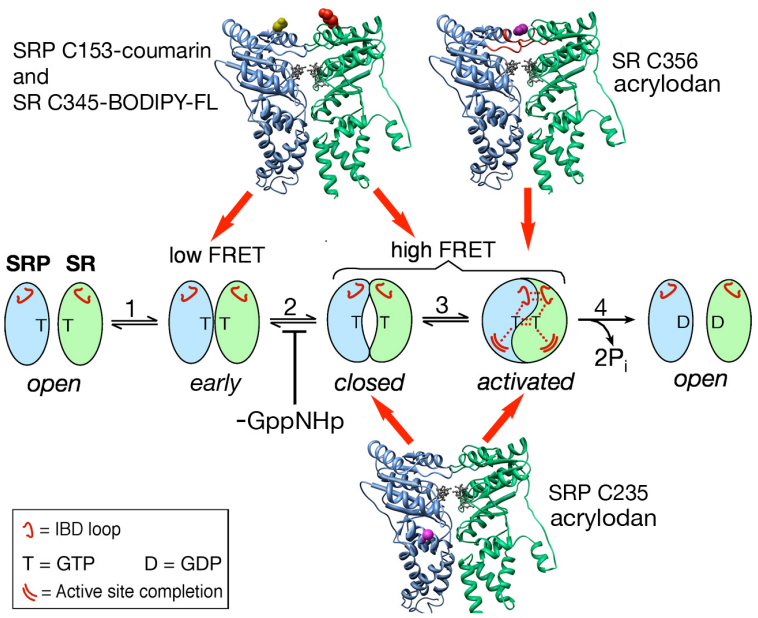

Figure 4.1. Multiple conformational changes during SRP-SR complex formation and activation (*9, 80*), as described in the text, and the positions of fluorescence probes that detect the different conformational stages, as described in the text.

4.3.2 Cargo Accelerates Assembly of a Stable SRP•SR Complex over 100 Fold

As cargo, we purified stalled ribosome•nascent chain complexes (RNCs) bearing the N-terminal 74 amino acids of the model SRP substrate FtsQ (*67, 81, 82*). SRP–SR complex assembly was monitored using FRET in the presence of GppNHp. Comparison of the time courses for complex assembly shows three differences between free and cargo-loaded SRP (figure 4.2*A*): (1) the initial rates are much faster with cargo-loaded SRP; (2) the kinetics of complex formation with cargo-loaded SRP is bi-phasic with a burst phase, suggesting the accumulation of an intermediate; (3) at completion of the reaction, FRET plateaus at a lower value for cargo-loaded SRP, suggesting a change in the equilibrium stability of the final SRP•SR complex. These effects are further characterized in the following.

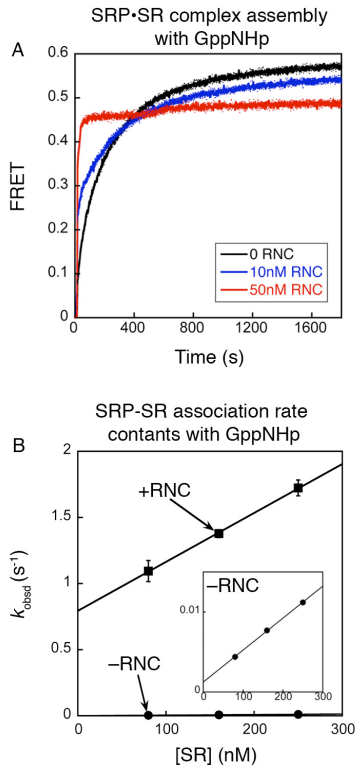

Figure 4.2. Cargo changes the kinetics of SRP-SR interaction. (*A*) Time courses for SRP-SR complex assembly with GppNHp in the absence (black) or presence of 10 nM (blue) and 50 nM (red) RNC, using 10 nM SRP and 100 nM SR to mimic physiological protein concentrations (*83*). (*B*) Cargo accelerates SRP–SR complex assembly with GppNHp by 100 fold. The data are fit to the equation: $k_{obsd} = k_{on}[SR] + k_{off}$, and gave association rate constants (k_{on}) of $3.7 \pm 0.4 \times 10^6$ M^{-1} s^{-1} and $4.0 \pm 0.3 \times 10^4$ M^{-1} s^{-1} with (■) and without (●) 60 nM RNC, respectively.

An observed rate constant for complex formation (k_{obsd}) at any protein concentration is the sum of the complex assembly and disassembly rate constants (*84*)

$$k_{obsd} = k_{on} \times [SR] + k_{off} \ . \qquad (4.1)$$

To isolate the effect of cargo on complex assembly, we measured the observed rate constants as a function of SR concentration; the slope of this concentration dependence gives the association rate constant, k_{on} [Eq. (4.1); figure 4.2*B*]. The value of k_{on} is 4.4×10^4 $M^{-1}s^{-1}$ in the absence of cargo, consistent with previous measurements (*21*). In the

presence of cargo, the complex formation rate constant is 100–400 fold faster (figure 4.2*B* and figure 4.S3A). Thus cargo-loaded SRP has a substantial kinetic advantage over free SRP to form a complex with the SR, ensuring efficient delivery of cargo to the target membrane.

4.3.3 Cargo Stabilizes the *Early* Intermediate by Two Orders of Magnitude

The biphasic kinetics with a burst phase during complex formation with cargo-loaded SRP suggests the accumulation of an intermediate (figures 4.2*A* and 4.3*A*, blue). A likely candidate to account for this burst is the *early* intermediate, which forms quickly and has a lower FRET value than the subsequent complexes (figure 4.1) (*80*). To test this notion, we blocked the *early* $\rightarrow$ *closed* rearrangement and isolated the *early* complex by performing complex assembly in the absence of nucleotide (figure 4.1, step 2; figure 4.3*A*, green). Both the rate and the magnitude of FRET changes for assembly of the *early* intermediate agree well with those of the burst phase during complex assembly with GppNHp (figure 4.3*A*). This provides strong evidence that in the presence of cargo, the *early* intermediate accumulates substantially during complex assembly.

The *early* intermediate, which lacks stabilizing interactions from the γ-phosphate of GTP, is very unstable without cargo (*26, 80*), hence it cannot accumulate under the nanomolar concentrations of SRP and SR used here (figure 4.2*A*, black). Therefore it was surprising to detect its accumulation with cargo-loaded SRP. This observation suggests that the cargo strongly stabilizes this intermediate. To test this hypothesis, we determined the equilibrium and kinetic stability of the *early* complex with and without cargo. Indeed, the cargo stabilizes the *early* complex over 50 fold, lowering its

equilibrium dissociation constant (K_d) from 4–10 microM (*80*) to 80 ± 4 nM (figure 4.3*B*, squares) and decreasing its dissociation rate constant (k_{off}, derived from the y-intercept in figure 4.3*C*) from 62 ± 2 s^{-1} to 1.6 ± 0.1 s^{-1}.

Stabilization of the *early* intermediate explains the faster rate of SRP–SR complex assembly with GppNHp for cargo-loaded SRP (figure 4.2*B*). Without cargo, formation of the highly labile *early* intermediate is not sufficient to give a stable SRP•SR complex; to obtain a stable complex, the *early* intermediate needs to rearrange to the *closed* complex. However the *early* intermediate dissociates quickly and less than 2% of the population rearranges to form the *closed* complex (k_{off} = 62 ± 2 s^{-1} *vs* $k_{rearrange}$ = 1.03 ± 0.02 s^{-1}) (*80*). This gives rise to the slow rate constant for formation of a stable *closed* complex between free SRP and SR. In contrast, for cargo-loaded SRP the *early* intermediate is stabilized over 50 fold. Thus forming the *early* complex (figure 4.1, step 1) is sufficient to give a relatively stable SRP•SR complex under physiological SRP and SR concentrations (200–400 nM) (*83*). Furthermore, the cargo•SRP•SR *early* complex dissociates with much slower kinetics (figure 4.3*C*, k_{off} = 1.6 ± 0.1 s^{-1}), giving this intermediate a much longer lifetime to undergo subsequent rearrangements. Both of these effects contribute to the faster rate of assembling a stable GTPase complex with cargo-loaded SRP in the presence of GppNHp.

4.3.4 Cargo Stalls the SRP•SR Complex at Earlier Conformational Stages

The different FRET end points in figure 4.2*A* suggest that the stability of the final SRP•SR complex is also altered by the cargo. To test this hypothesis, we compared the equilibrium stability of the SRP•SR complex assembled in GppNHp with and without

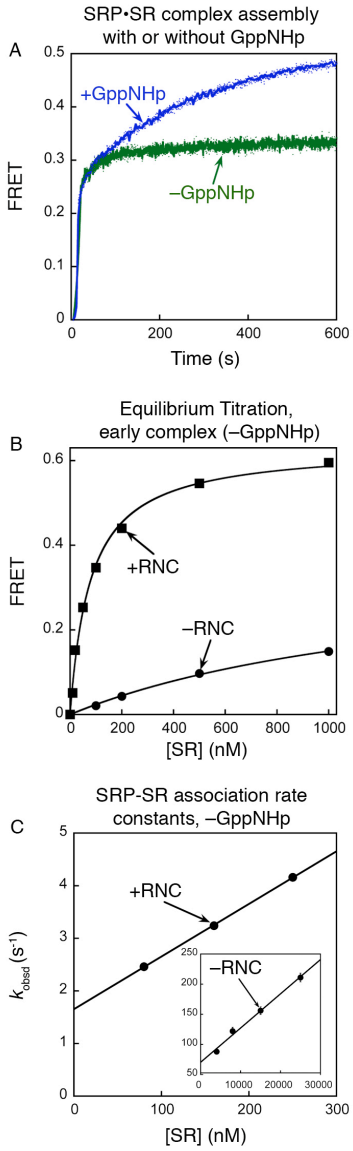

Figure 4.3. Cargo stabilizes the early intermediate. (*A*) Comparison of the time courses for SRP–SR complex formation for cargo-loaded SRP in the absence (green) and presence of 100 microM GppNHp (blue). Data were obtained using 20 nM SRP, 100 nM SR and 20 nM RNC. (*B*) Cargo stabilizes the *early* intermediate 50 fold. Equilibrium titration of the *early* complex assembled in the absence of GppNHp with (■) and without (●) 50 nM RNC. Nonlinear fits of data gave K_d values of 80 ± 4 nM in the presence of RNC. (*C*) Cargo increases the kinetic stability of the *early* intermediate 40 fold. The data are analyzed as in part B and give $k_{on} = 1.0 \pm 0.1 \times 10^7$ M^{-1} s^{-1} with cargo-loaded SRP, which is within two fold of the value in the absence of RNC ($k_{on} = 5.6 \pm 0.3 \times 10^6$ M^{-1} s^{-1}) (*80*), and $k_{off} = 1.62 \pm 0.1$ s^{-1}, which is 40 fold slower than that in the absence of RNC ($k_{off} = 60 \pm 2$ s^{-1}) (*80*). The inset shows the data in the absence of RNC (adapted from ref. (*80*)). Note the difference in scales between the two plots.

cargo using SRP C235 labeled with acrylodan (figure 4.1 and figure 4.S1). Equilibrium titrations using this probe showed that the cargo destabilizes the *closed/activated* complexes four fold, increasing its K_d from 10 ± 2 nM to 40 ± 4 nM (figure 4.4*A*). A similar destabilizing effect was observed using the FRET probes, with the K_d of the *closed/activated* increasing from 14 ± 3 nM without cargo to 60 ± 7 nM with cargo-loaded SRP (figure 4.S4). An additional probe that specifically monitors the *activated* complex, acrylodan-labeled SR C356 (figure 4.1 and figure 4.S2), also confirmed that the cargo destabilizes the *activated* complex (figure 4.4*B*). In summary, the results from all three fluorescence probes showed that, in contrast to the large stabilizing effect of the cargo on the *early* intermediate, the subsequent conformations during the SRP-SR interaction are destabilized by the cargo.

Thus the cargo significantly alters the conformational rearrangements in the SRP•SR complex (figure 4.4*C*). Without cargo, the *closed* and *activated* states are >400 fold more stable than the *early* intermediate, therefore the equilibrium for the *early* → *closed* rearrangement is extremely favorable (figure 4.4*C*, $K^{rel} = 400$). In contrast, in the cargo•SRP•SR complex this rearrangement is 200 fold less favorable (figure 4.4*C*, K^{rel} = 1.3–2). Thus in the cargo•SRP•SR complex, a substantial fraction of the GTPase complex is still in the *early* conformation (30–40%) even in the presence of GppNHp. This conformational heterogeneity of the GTPase complex in the presence of cargo is consistent with previous EM analysis that showed that, while the SRP is well-resolved in the RNC•SRP complex, upon addition of SR and GppNHp the electron density for both the SRP and SR's GTPase domains are no longer visible (*85*). Thus both the biochemical

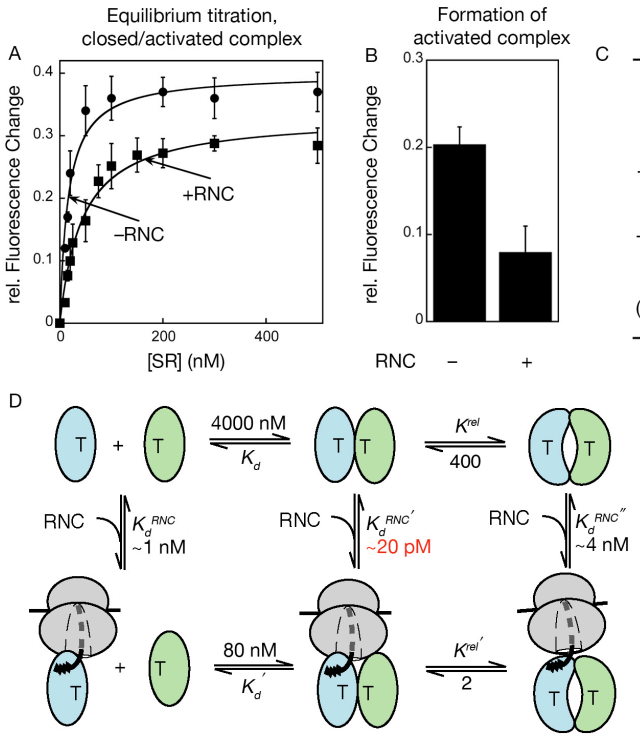

Figure 4.4. Cargo destabilizes the *closed* and *activated* states during SRP–SR interaction. (*A*) Equilibrium titration of the SRP•SR complex assembled in GppNHp with (■) and without (●) RNC using acrylodan-labeled SRP C235. Nonlinear fits of data gave K_d values of 10 ± 2 nM (without RNC) and 40 ± 4 nM (with RNC). (*B*) Relative fluorescence changes of acrylodan-labeled SR C356 in the presence and absence of cargo, obtained using 50 nM SRP and 15 nM labeled SR with 100 microM GppNHp. An accurate K_d value could not be determined with this probe because of the large amount of cargo-loaded SRP that would be required to saturate labeled SR C356. (*C*) Equilibrium constants of the GTP-independent (K_d^{-G}) and GTP-dependent (K_d^{+G}) SRP•SR complexes with or without RNC. The equilibrium for rearrangement (K^{rel}) were calculated from $K^{rel} = K_d^{-G}/K_d^{+G}$. (*D*) Thermodynamic analysis of the interaction of cargo with SRP at different conformational stages during the SRP–SR interaction.

and structural analyses highlight the dynamic nature of the GTPase complex when it is bound to the cargo.

The SRP•SR complex can use the *early* → *closed* rearrangement to drive cargo unloading during protein targeting (figure 4.4*D*). Initially, cargo loading stabilizes the *early* intermediate 50 fold (figure 4.4*D*, K_d and K_d'). Correspondingly, the interaction of

cargo with SRP should be stabilized to the same extent in the *early* intermediate (figure 4.4*D*, $K_d^{RNC\prime}/K_d^{RNC} = K_d\prime/K_d = 50$). Using the value of $K_d^{RNC} \sim 1$ nM (*86, 87*), the stability of cargo bound to the *early* intermediate would be in the range of $K_d^{RNC\prime} \sim 20$ pM. Although this effect could enhance the initial recognition and delivery of cargo to the membrane, such strong binding will block the subsequent unloading of cargo from the SRP. This problem is circumvented by the 200 fold destabilizing effect of cargo on the *early* → *closed* rearrangement (figures 4.4*C* and 4.4*D*, K^{rel} and $K^{rel\prime}$). Correspondingly, the interaction of cargo with SRP would also be weakened 200 fold by this rearrangement (figure 4.4*C*, $K_d^{RNC\prime\prime}/K_d^{RNC} = K^{rel\prime}/K^{rel}$), thus priming the cargo for subsequent unloading. This model is supported by mutational analyses that showed that mutant GTPases defective in the *early* → *closed* rearrangement severely block protein translocation (*10*). The observation that mutants defective in the *closed* → *activated* rearrangement inhibit protein translocation further suggest that this last rearrangement is also essential for cargo unloading (*10*). Therefore both rearrangements within the GTPase complex provide essential driving forces to help unload the cargo from the SRP to the PCC, thus initiating protein translocation.

Since cargo disfavors the rearrangements to form the *activated* complex, one would predict that stimulated GTP hydrolysis, which occurs from the *activated* complex, would also be impaired. To test this notion, we compared the GTPase reaction rate from the SRP•SR complex in the presence and absence of cargo. In the absence of cargo, the GTPase rate of free SRP is significantly stimulated by the addition of SR (figure 4.5, circles). The reaction rate reaches a plateau of 0.79 s^{-1} at saturating SR concentrations,

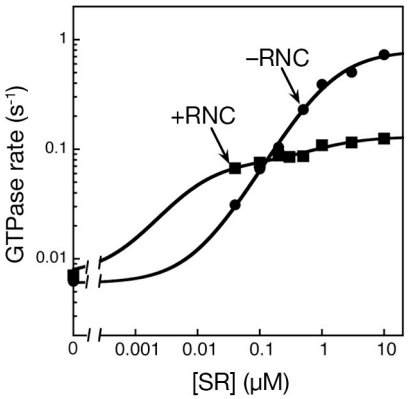

Figure 4.5. Cargo delays activation of GTP hydrolysis in the SRP•SR complex. GTPase rate constants were measured using 40 nM SRP and 100 microM GTP in the absence (●) and presence (■) of 100 nM RNC. The data in the absence of cargo were fit to a single binding curve and gave a rate constant of 0.79 s^{-1} for GTP hydrolysis from the SRP•SR complex. The data in the presence of cargo is not consistent with a single binding curve and was fit to a model based on two populations of SRP•SR complexes that reacts at rate constants of 0.064 and 0.11 s^{-1}.

representing the GTPase rate constant from the SRP•SR complex (figure 4.5, circles). In the presence of cargo, significantly less GTPase stimulation was observed (figure 4.5, squares). Intriguingly, two plateaus were observed for the GTPase reaction in the presence of cargo (figure 4.5, squares), suggesting the presence of two populations of cargo•SRP•SR complexes: one population, which forms at low SR concentrations (below 50 nM), hydrolyzes GTP at a rate constant of 0.064 s^{-1}; the second population, which forms at higher SR concentrations (above 1 microM), hydrolyzes GTP at a rate constant of 0.11 s^{-1} (figure 4.5, squares). Although the nature of this heterogeneity is unclear at present, in both of these populations the GTPase activity is repressed by the RNC (12- and 8 fold for the first and second population, respectively). The effect of cargo in reducing the GTP hydrolysis rate is specific to the SRP•SR complex, as the cargo does not affect the basal GTP hydrolysis rate of free SRP (figure 4.S5). Thus the cargo also

delays GTPase activation in the SRP•SR complex. This effect, which we term 'stalling', would provide an important time window that allows the SRP to unload the cargo before GTP hydrolysis drives irreversible complex disassembly, as discussed below.

4.4 Discussion

We showed here that cargo loading substantially alters the free energy landscape of the SRP–SR interaction cycle (figure 4.6*A*). Without cargo (black), assembly of a stable SRP•SR complex is slow because it requires rearrangement from an unstable *early* intermediate (figure 4.6A, $\Delta G^{\ddagger}_{complex} = \Delta G_{early} + \Delta G^{\ddagger}$) (*80*). Further, the stable SRP•SR complex has a short lifetime because as soon as it is formed, rapid activation of GTP hydrolysis drives its irreversible disassembly (*29*). The cargo uses a remarkably simple solution to these problems, by stabilizing the *early* intermediate (figure 4.6*A*, $\Delta\Delta G = -2.4$ kcal/mol) and disfavoring the *closed* and *activated* states (figure 4.6*A*, $\Delta\Delta G \geq +0.8$ kcal/mol). This accelerates complex assembly (figure 4.6*A*, $\Delta\Delta G^{\ddagger} = -2.8$ kcal/mol), and prolongs the lifetime of the SRP•SR complex due to delayed GTP hydrolysis (figure 4.6*A*, $\Delta\Delta G^{\ddagger} = +1.3 - 1.5$ kcal/mol). The rate-limiting step of the SRP–SR interaction cycle shifts from the *early* → *closed* rearrangement with free SRP to GTP hydrolysis with cargo-loaded SRP.

These cargo-induced effects allow the SRP and SR to use each of their conformational rearrangements to regulate a distinct step during protein targeting (figure 4.6*B*). At the beginning of each targeting cycle, cargo loading (figure 4.6*B,* step 1) allows the SRP to assemble a stable complex with SR >100 fold faster (figure 4.6*B,* step 2). This ensures rapid delivery of cargo to the membrane (*88, 89*), and avoids futile

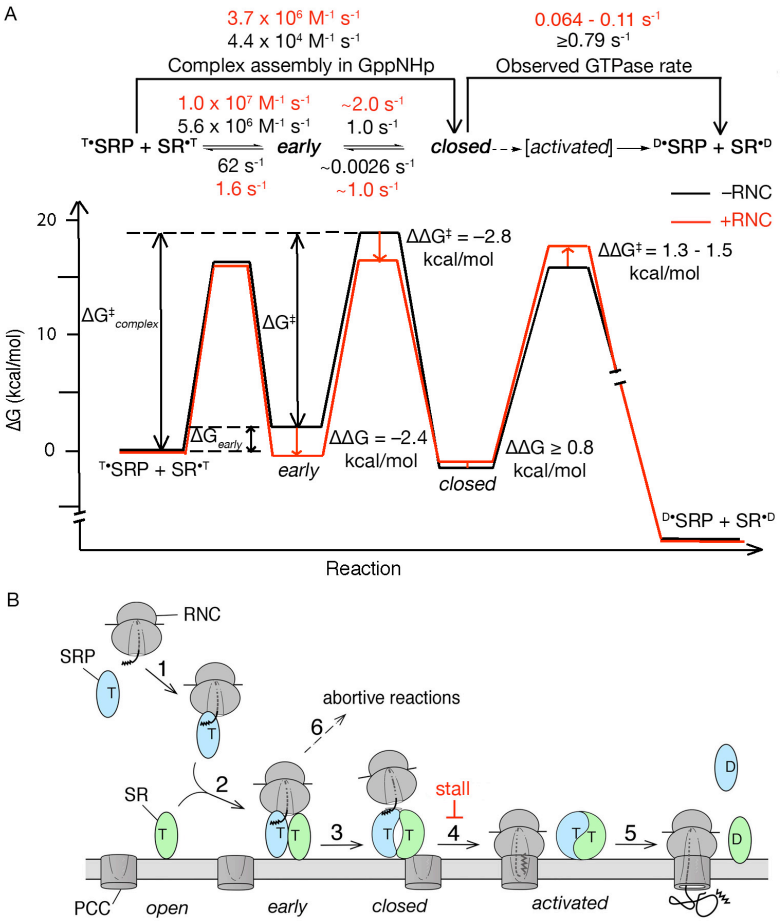

Figure 4.6. Conformational changes during the SRP–SR interaction respond to cargo loading and regulate protein targeting. (*A*) Rate constants and free energy profile for the SRP–SR interaction in the absence (black) and presence (red) of cargo. A standard state of 200 nM SRP is used to approximate cellular protein concentrations. Activation energies were calculated from the observed association and dissociation rate constants using $\Delta G^{\ddagger} = -RT \ln(kh/k_BT)$, where R = 1.987 cal K^{-1} mol^{-1}, $h = 1.58 \times 10^{-37}$ kcal s^{-1}, $k_B = 3.3 \times 10^{-27}$ kcal K^{-1}, and T = 298K. The relative energies of the different complexes were calculated from the observed equilibrium stabilities using $\Delta G = -RT \ln K$, where K is the equilibrium constant. ΔG_{early} is the free energy cost to form the *early* complex, $\Delta G^{\ddagger}$ is the activation energy for the *early* → *closed* rearrangement. The sum of these two gives the overall energy barrier to form the *closed* complex ($\Delta G^{\ddagger}_{complex}$), which is lowered 2.8 kcal mol^{-1} by the cargo because the cargo stabilizes the *early* complex by 2.4 kcal mol^{-1}. In contrast, the RNC increases the activation energy for GTP hydrolysis by 1.9 kcal mol^{-1}. (*B*) Proposed model for how the conformational changes during the SRP–SR interaction regulate protein targeting and translocation as described in text.

interactions between free SRP and SR. In the *early* intermediate, the cargo is locked in the SRP•SR complex with very high affinity (figure 4.4D, $K_d^{RNC\prime} \sim 20$ pM), allowing the SRP to effectively compete with cellular chaperones for binding the cargo. Subsequent GTPase rearrangements to the *closed* and *activated* conformations weaken the interaction of cargo with the SRP (figure 4.6*B,* steps 3–4; and figure 4.4*D*) and thus help the SRP to switch from a cargo-binding mode to a cargo-release mode, to unload the cargo to the PCC (figure 4.6*B,* step 4). Once in the *activated* conformation, and especially after cargo release, rapid GTP hydrolysis drives the disassembly and recycling of SRP and SR (figure 4.6*B,* step 5).

The mechanism proposed here (figure 4.6*B*) focuses on GTP-bound SRP and SR because the high cellular concentration of GTP compared to GDP (~900 microM and 100 microM in bacteria, respectively) predicts that over 90% of both GTPases are bound with GTP. Minor pathways are also possible in which empty-site or GDP-bound forms of SRP and SR first form the *early* intermediate to deliver cargo to the membrane surface, followed by rapid binding or exchange of GTP to drive the subsequent steps (*88, 89*); these pathways are not depicted in Figure 4.6*B* for clarity.

The most intriguing effect of cargo is 'stalling', i.e., the delay of GTPase activation by ~8–12 fold (figure 4.6*B*, step 4). A similar effect was suggested from studies of the mammalian system where prior to the addition of the PCC, a stable cargo•SRP•SR complex persists in the presence of GTP, suggesting that the cargo may also delay GTP hydrolysis in the mammalian SRP•SR complex (*90*). We suggest that stalling creates an important time window during which SRP ensures the efficiency and fidelity of protein targeting, via either or both of the following mechanisms. First,

stalling could provide a spatial checkpoint for the target membrane and/or the PCC. Before the SR associates with the PCC, stalling prevents premature GTP hydrolysis that would irreversibly disassemble the SRP•SR complex, and thus help avoid abortive targeting reactions (figure 4.6*B*, step 6). Interaction of SR with the PCC may trigger the rearrangement to the *closed* and *activated* states and initiate cargo unloading (*90*). The PCC also competes with SRP for interacting with the RNC (*81, 82, 85, 91*), which could further drive the transfer of cargo from SRP to the PCC (*90, 92*). Alternatively, stalling could provide a fidelity checkpoint. Many of the effects of the cargo described here are observed only with RNCs but not with empty ribosomes (figure 4.S6) nor with RNCs bearing weak signal sequences, establishing the importance of the signal sequence. It could be envisioned that cargos with weaker signal sequences could not effectively stall the SRP•SR complex, and thus are more likely to be rejected via premature GTP hydrolysis (figure 4.6*B*, step 6). In this way, GTP hydrolysis could be used to improve the fidelity of protein targeting akin to kinetic proofreading mechanisms used by elongation factor (*93*).

4.5 Materials and Methods

4.5.1 Materials

The *Eschericia coli* SRP and SR GTPases (Ffh and FtsY, respectively) and 4.5S RNA were expressed and purified using established procedures (*10, 29*). Most of the fluorescence experiments used the FtsY(47 –497) construct. This truncated FtsY construct behaves similarly to full length FtsY in its ability to interact with the SRP and to respond to the cargo (SI: figure S3). The GTPase reactions with and without cargo was determined with full length FtsY. Mutant proteins were constructed using the QuickChange procedure (Stratagene, La Jolla, CA), and were expressed and purified by the same procedure as that for the wild-type protein. Fluorescent dyes DACM, BODIPY-FL and acrylodan were from Invitrogen (Carlsbad, CA). 70S ribosomes and RNCs were purified as described previously (*67, 94, 95*).

4.5.2 Fluorescence labeling

For FRET measurements, maleimide derivatives of coumarin and BODIPY-FL were used to label single-cysteine mutants of SRP and SR, respectively, as described (*80*). Labeling of SRP and SR with acrylodan followed the same procedure except that the labeling reaction was carried out using a 30 fold excess of dye over protein for over twelve hours at 4 ºC. Absorbance of acrylodan (e_{391} = 20,000 M^{-1} cm^{-1}) was used to determine the concentration of labeled protein. The efficiency of labeling reaction was typically ≥90% for both proteins. The background, estimated from the labeling of cysteinless SRP and SR using the same procedure, is less than 3%.

4.5.3 Fluorescence measurement

All measurements were carried out at 25 °C in assay buffer [50 mM KHEPES, pH 7.5, 150 mM KOAC, 10 mM $Mg(OAc)_2$, 2 mM DTT, 0.01% Nikkol] on a Fluorolog-3 spectrofluorometer (Jobin Yvon, Edison, NJ) as described (*29, 80*). FRET measurements were carried out using an excitation wavelength of 380 nm and an emission wavelength of 470 nm. FRET efficiency was calculated as described (*80*). Fluorescence emission spectrum of SRP (or SR) labeled with acrylodan was measured using an excitation wavelength of 370 nm. Fluorescence emission at 500 nm was monitored for equilibrium titrations using acrylodan-labeled protein.

Pulse chase experiments were carried out using unlabeled protein to trap any dissociated protein SRP or SR (*21*). Fast reactions were measured on a Kintek stop-flow apparatus (*21*). The incubation time during equilibrium measurements was calculated based on the SRP•SR complex assembly rate (*21, 80*), and varies from five minutes for fast reactions (*early* complex assembly and complex assembly in the presence of cargo) to several hours (complex assembly with GppNHp in the absence of cargo).

4.5.4 GTPase assay

The GTPase assay to measure the stimulated GTP hydrolysis reaction between SRP and SR were carried out and analyzed as described (*29*). Multiple turnover reactions were carried out at 25 °C with a small, fixed amount of free or cargo-loaded SRP and increasing concentrations of SR, 100 microM GTP (doped with trace γ-^{32}P-GTP) was present in the reaction to saturate both GTPase sites. Previous studies have established that the GTPase reaction rate is ratelimited by SRP-SR complex formation at

subsaturating SR concentrations, whereas at saturating SR concentrations, the reaction is rate-limited by GTP hydrolysis or a slow conformational change preceding GTP hydrolysis (*29*). The release of products, including dissociation of GDP, P_i, and disassembly of the ^{GDP}•SRP•SR$^{•GDP}$ complex, are not ratelimiting for the GTPase assay (*29*).

4.5.5 Preparation of 70S ribosomes and RNCs

70S empty ribosomes were purified from *E coli* MRE600 following a modified protocol described by Moazed and Noller (*95*). Cell pellet from a 1 L culture was resuspended in 30 mL buffer A [20 mM Tris•HCl (pH 7.0 at 21 ºC), 10.5 mM $MgCl_2$, 100 mM NH_4Cl, 0.5 mM EDTA, 6 mM 2-mercapto ethanol (βME)]. The cell resuspension was passed through the French Press twice to lyse the cells. The lysate was clarified by two rounds of centrifugation at 20,000 g for 15 minutes at 4ºC. The supernatant was layered on a 1.1 molar sucrose cushion in buffer B [20 mM Tris•HCl (pH 7.0 at 21 ºC), 10.5 mM $MgCl_2$, 500 mM NH_4Cl, 0.5 mM EDTA, 6 mM βME, 1.1M sucrose] and ultracentrifuged at 100,000 g for 21 hours at 4ºC. The ribosome pellet was collected and dissolved in buffer A containing 500 mM NH_4Cl. The dissolved ribosomes were ultracentrifuged at 4 ºC for 3 hours at 100,000 x g. The pellet was dissolved in buffer C [20 mM Tris•HCl (pH 7.0 at 21 ºC), 6 mM $MgCl_2$, 100 mM NH_4Cl, 6 mM βME], layered on top of 32 mL sucrose gradients (10%-40% w.v. sucrose in buffer C), and ultracentrifuged at 50,000 x g for 14 hours at 4ºC. Fractions containing 70S ribosomes were collected and ultracentrifuged at 100,000g for 17 hours at 4 ºC. Ribosome pellets were collected and dissolved in storage buffer [20 mM Tris•HCl (pH

7.0 at 21ºC), 10 mM $MgCl_2$, 100 mM NH_4Cl, 6mM βME]. Ribosomes were stored at -80ºC.

The RNC was generated from *in vitro* translation in a membrane-free cell extract prepared from *E. coli* MRE600 as described (*67*). I*n vitro* translation was performed at 37ºC for 25 minutes. The translation mix was layered onto a 40 mL sucrose gradient in buffer S1 (10-50% w.v. sucrose in 50 mM HEPES-KOH (pH 7.5 at 4 ºC), 100 mM $Mg(OAc)_2$, 100 mM NH_4Cl) and ultracentrifuged at 4 ºC for 15 hours at 23,500 rpm using a SW-32 rotor (Beckman). Fractions containing monoribosome were collected and loaded onto a 1 mL Strep-Tactin sepharose column (IBA, Göttingen Germany) equilibrated with buffer S1 at 4 °C. Buffer S1 containing 2.5 mM desthiobiotin (Sigma) was used to elute RNCs from affinity column. RNC-containing fractions were centrifuged at 55,000 rpm for 3 hours at 4 ºC using a TLA-55 rotor (Beckman). Pellets were collected and dissolved in buffer S1 with 25 mM $Mg(OAc)_2$.

4.6 Supplementary Figures and legends

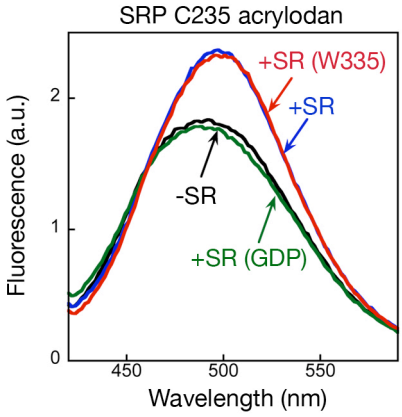

Figure 4.S1. Acrylodan labeled SRP C235 monitors formation of the *closed/activated* conformation. Fluorescence emission spectra are acquired in the presence of GppNHp for acrylodan-labeled SRP C235 alone (0.1 microM; black), labeled SRP C235 incubated with 1 microM wild type SR (blue), or labeled SRP C235 incubated with 1 microM SR A335W (red), which is blocked in the *closed* → *activated* rearrangement and thus isolates the *closed* complex (*9*), or in the presence of GDP with 10 microM SR (green), which isolates the *early* complex (*80*).

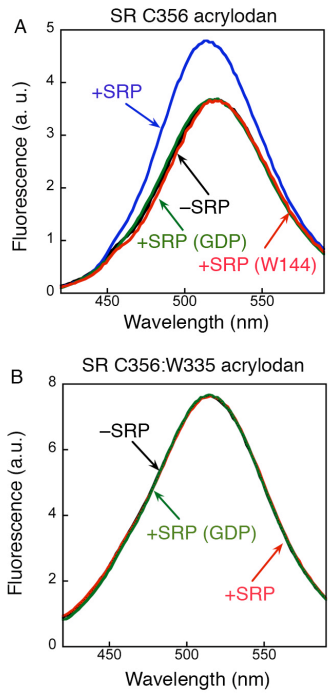

Figure 4.S2**.** Acrylodan labeled SR C356 specifically monitors formation of the *activated* SRP•SR complex. (*A*) Fluorescence emission spectra was obtained for acrylodan labeled SR C356 alone (0.1 microM; black), acrylodan labeled SR C356 incubated with wild type SRP (blue) or SRP A144W (red) in the presence of GppNHp, or with 10 microM SRP in the presence of GDP (green). SRP A144W allows a stable *closed* complex to form but specifically blocks formation of the *activated* complex (*10*). The absence of fluorescence change with SRP A144W shows that acrylodan labeled SR C356 specifically monitors formation of the *activated* complex. (*B*) Acrylodan labeled C356 does not change fluorescence if mutant SR A355W (*9*) was used to block the formation of the *activated* complex. Spectra was obtained for 0.1 microM acrylodan labeled SR A335W:C356 alone (black) and when this labeled SR mutant was incubated with 1 microM SRP in the presence of GppNHp (red) or with 5 microM SRP in the presence of GDP (green). The absence of a fluorescence change shows that the probe on SR T356 does not detect the *early* or the *closed* complex.

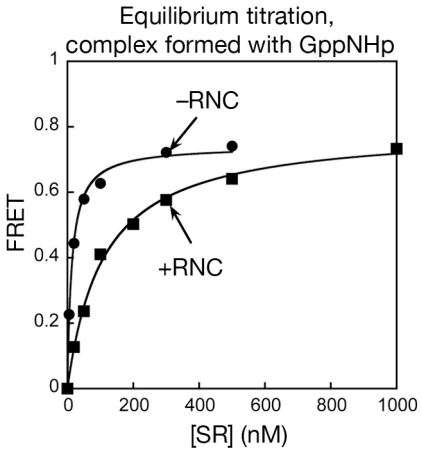

Figure 4.S3. Equilibrium titration of the SRP•SR complex assembled in GppNHp with (■) and without (●) RNC using the FRET assay. Nonlinear least squares fits of data gave K_d values of 14 ± 3 nM (without RNC) and 60 ± 7 nM (with RNC). For cargo-loaded SRP, an accurate determination of the stability of the *closed/activated* states by FRET is complicated by the fact that the stabilities of the SRP•SR complexes assembled with and without GppNHp are very similar (60 vs. 80 nM, respectively), thus a significant fraction of the SRP•SR complex is in the *early* conformation even in the presence of GppNHp. The observed affinity of the cargo•SRP•SR complex of 60 nM is consistent with the weighted average of the stabilities of the *early* intermediate (80 nM, figure 4.4*C*) and the *closed* complex (40 nM, figure 4.4*C*) that are equally populated in the presence of GppNHp and cargo.

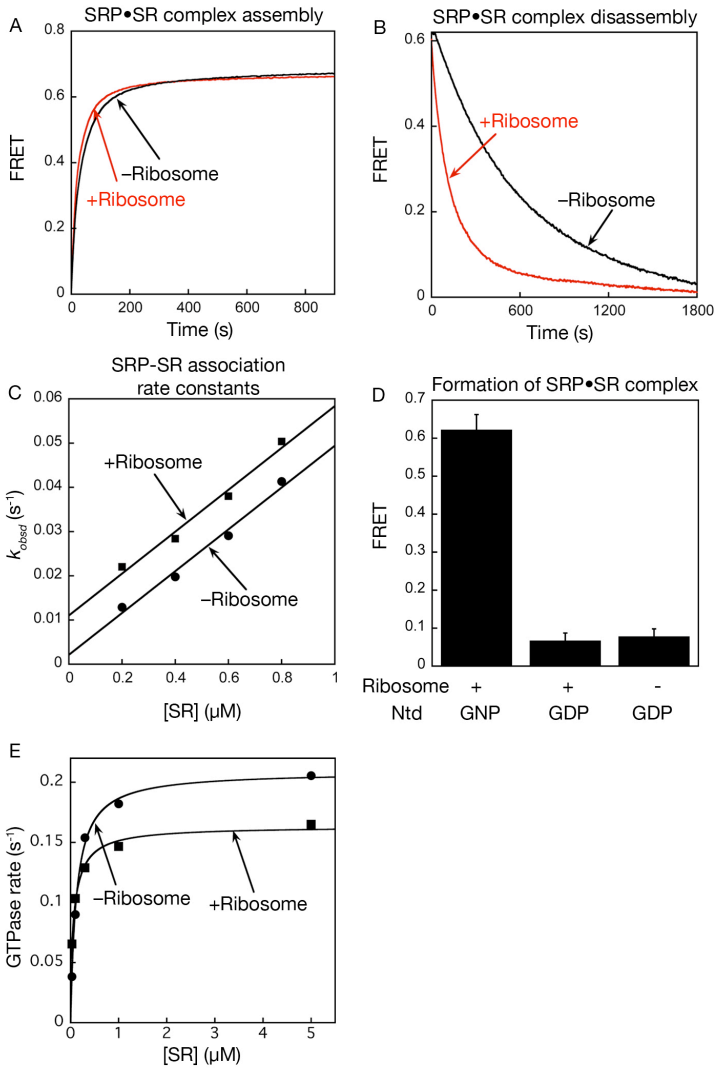

Figure 4.S4. Empty ribosomes do not substantially alter the interaction between SRP and SR. (*A*) The time course for SRP–SR complex formation, monitored by FRET, in the absence (black) and presence (red) of 0.8 microM ribosomes. Data were obtained with 0.1 microM SRP, 1.0 microM SR, and 100 microM GppNHp. (*B*) The ribosome accelerates disassembly of the SRP•SR complex ~ 3 fold. The rate constants for complex disassembly were determined in the absence (black) and presence (red) of 1.0 microM ribosomes. Fits of the data to single exponential decay give dissociation rate constants of 0.010 ± 0.003 s^{-1} and 0.0027 ± 0.004 s^{-1} in the presence and absence of ribosome, respectively. (*C*) The ribosome does not affect the rate of SRP–SR complex assembly. Association kinetics of the SRP•SR complex was measured as in figure 4.2 with (■) or without (●) 1.0 microM ribosome. Linear fits of the data gave k_{on} values of $4.7 \pm 0.7 \times 10^4$ M^{-1} s^{-1} with ribosome and $4.7 \pm 0.4 \times 10^4$ M^{-1} s^{-1} without ribosome, and k_{off} values of 0.011 ± 0.004 s^{-1} with ribosome and 0.0022 ± 0.003 s^{-1} without ribosome. (*D*) Ribosome does not stabilize the *early* intermediate. FRET values are compared for SRP•SR *early* complex assembled with GDP in the presence and absence of ribosome. Data are obtained with 0.1 microM SRP, ribosome, and 1.0 microM SR. (*E*) Ribosome does not

substantially affect the stimulated GTP hydrolysis on the SRP•SR complex. GTPase rate constants were measured and analyzed as described in Methods using 15 nM SRP and 50 microM GTP in the absence (●) and presence (■) of 1.0 microM ribosome.

4.7 Acknowledgments

We thank Sandra Schmid, Douglas C. Rees, Raymond Deshaies, Nathan Pierce, and members of the Shan laboratory for comments on the manuscript. This work was supported by NIH grant GM078024 to S.S., and by the Swiss National Science Foundation (SNSF) and the NCCR Structural Biology program of the SNSF to N.B.. S.S. was supported by a career award from the Burroughs Welcome Foundation, the Henry and Camille Dreyfus foundation, the Beckman Young Investigator award, and the Packard and Lucile award in science and engineering. X.Z. was supported by a fellowship from the Ulric B. and Evelyn L. Bray Endowment Fund